European Journal of Radiology Open 3 (2016) 254–258

Contents lists available at ScienceDirect

European Journal of Radiology Open

journal homepage: www.elsevier.com/locate/ejro

Dual-energy CT of liver metastases in patients with uveal melanoma

Jens Altenbernd*, Axel Wetter, Michael Forsting, Lale Umutlu

Department of Diagnostic and Interventional Radiology and Neuroradiology, University Hospital Essen, Germany

ARTICLE INFO

Article history:
Received 29 August 2016
Accepted 22 October 2016
Available online 25 October 2016

Keywords:
Dual energy CT
Liver
Uveal melanoma
Angiography
Staging

ABSTRACT

Objective: To investigate the value of different kVp images of dual-energy CT (DECT) for the detection of liver metastases.

Methods: 20 Patients with uveal melanoma were investigated with DECT of the liver. In each patient contrast-enhanced DECT imaging with arterial delay was performed. Number and size of metastases were documented on arterial phase 80-kVp images, virtual 120-kVp images and following angiographic images (DSA) as part of hepatic chemoperfusion. Attenuation of metastases and several anatomic regions, subjective (image noise, image quality) and objective (SNR, CNR) parameters were documented.

Results: The mean number of liver metastases detected was significant higher on 80-kVp images than on virtual 120-kVp/DSA images (5.6 ± 2.1 vs. $4.1 \pm 1.8/4.3 \pm 1.6$); ($p < 0.001$). All lesions sizes were significant better detected with 80 kVp images than with virtual 120 kVp and DSA-Images (80 kVp vs. 120 kVp: <10 mm: 34 vs. 19, $p < 0.05$; 10–20 mm:, 33 vs. 25, $p < 0.05$; >20 mm: 56 vs. 42, $p < 0.05$/80 kVp vs. DSA: <10 mm: 34 vs. 18 $p < 0.05$; 10–20 mm: 33 vs. 24, $p < 0.05$; >20 mm: 56 vs. 41, $p < 0.05$). Number of detected small lesions <10 mm with 120 kVp compared to DSA-images were significant higher (19 vs. 13; $p < 0.05$), lesions 10–20 mm and >20 mm were measured statistically equally. Noise, SNR and CNR of 80 kVp images were higher compared to 120 kVp images. Image quality of 120 kVp images was higher compared to 80 kVp images.

Conclusion: Low-kVp images of DECT datasets are more sensitive in detecting liver metastases of patients with uveal melanoma than virtual 120 kVp- and DSA images.

1. Introduction

Uveal melanoma (UM) is a rare disease arising from the pigmented uveal tract of the eye. The incidence in Europe is 4.4 cases per million, varying between 2 in the south to 8 in the north of Europe [1]. Around 5% of patients with UM have distant metastases at diagnosis. Metastases appear usually within a median of 3 years after the treatment of the primary tumor with a range between 1 and 10 years. There is an unexplained hepato-tropism with the liver being the first site of metastases in up to 90% of patients and is the only site in 46% of them [2,3]

A recent development in CT has been the introduction of dual-source technology [4].

One important advantage of dual-source CT compared with a single-source system is the option to use the two tubes at different tube currents offering differentiation of materials of non-equal density. Previous study demonstrated the feasibility of contrast-enhanced dual-energy CT for the detection of hypervascular liver lesions in patients with hepatocellular carcinoma [5]. Higher detection rates were explained by higher attenuation of iodine in the low-kVp images in comparison to 140-kVp and virtual 120-kVp images.

FDG-PET-CT and MRI were described as reliable and accurate diagnostic methods in previous studies [6–9]. So far however, there is no study that investigated the sensitivity of the detection of hepatic metastases of uveal melanoma in DECT.

The aim of our study was to investigate to what extent the low kVp images of DECT are suitable compared to the virtual 120 kVp and DSA images for detection of liver metastases in patients with uveal melanoma. DECT was performed in each patient as part of the regular staging and planning examination before and 3 anf 6 monh after transarterial hepatic chemoperfusion. Angiographic image data sets were consulted as the reference imaging technique for comparison [10,11].

* Corresponding author at: Department of Diagnostic and Interventional Radiology and Neuroradiology, University Hospital Essen, Hufelandstrasse 55, 45122 Essen, Germany.
E-mail address: jens.altenbernd@uni-due.de (J. Altenbernd).

http://dx.doi.org/10.1016/j.ejro.2016.10.003

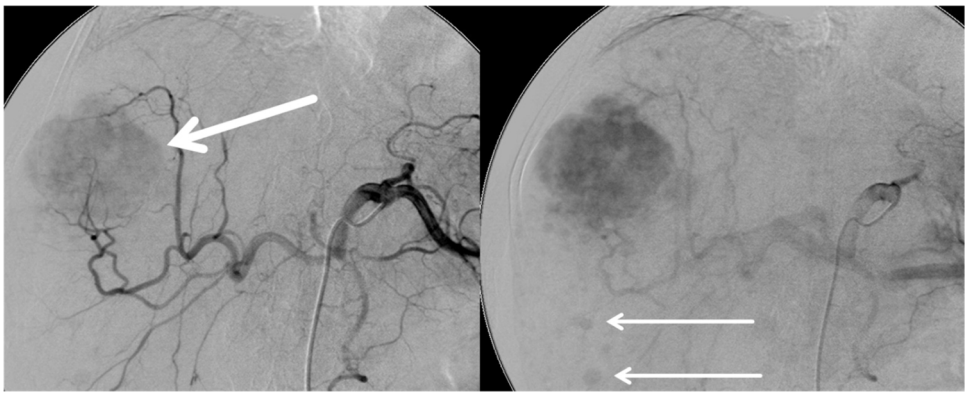

Fig. 1. Multiple hypervasculare liver metastases of uveal melanoma detected with DSA.

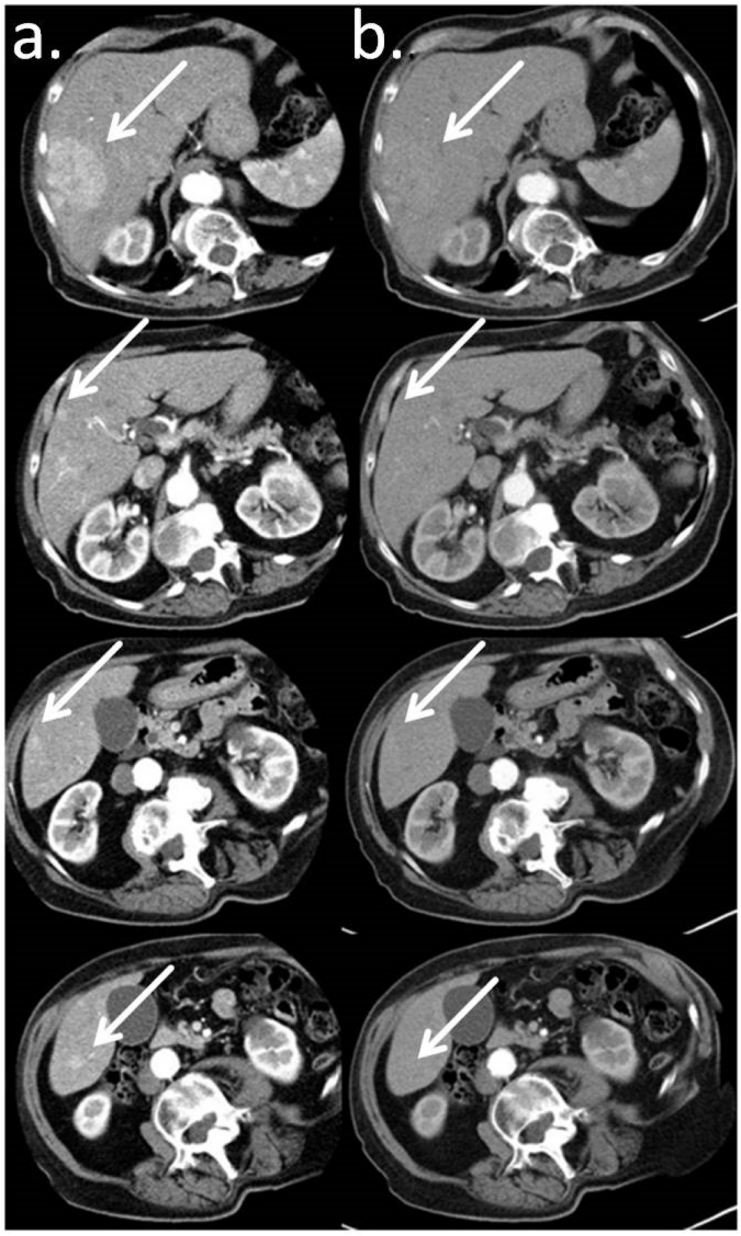

Fig. 2. Liver metastases of uveal melanoma detected significantly better on 80 kVp images (a) than on virtual 120 kVp (b) images based on DECT. (Slice thickness 3 mm; Window 350 HU, Center 50 HU, Kernel D50).

2. Materials and methods

2.1. Patient population

Between September 2009 and November 2011, 20 consecutive patients with uveal melanoma (13 men, 7 women; mean age 61 years ± 17 years) underwent dual-energy CT (DECT) for regular evaluation before transarterial chemoperfusion and 3 anf 6 months after therapy as regular follow up. The study was approved by our institutional review board and all patients provided written informed consent before participation (Figs. 1 and 2).

2.2. Imaging protocoll and parameters

All CT examinations were performed with a dual-source multidetector CT (Somatom Definition™ Dual Source; Siemens Medical Solutions, Forchheim, Germany). This system consists of two x-ray tubes mounted on one gantry at a 90° angle [4] and two corresponding 64-section detectors. One detector (detector A) covers a 50-cm field of view and the other detector (detector B) covers a 26-cm field of view [4]. Patients were positioned supine on the table. Patients were positioned slightly off centre to the left to ensure complete coverage of the liver by the smaller field of view of detector B. After intravenous injection of a non-ionic contrast agent (1.5 ml per kilogram of body weight, Xenetix 300™, *Guerbet, Sulzbach, Germany*) bolus tracking was started in the abdominal aorta at the level of the coeliac trunk. Dual-energy datasets were acquired in the arterial and portal venous (bolus tracking) phases from the dome of the liver to the iliac crest by operating tube A at 140 kVp and a reference value of 96 mAs and tube B at 80 kVp and a reference value of 404 mAs. For both tubes, an online dose modulation (Care DOSE 4D™, Siemens Medical Solutions) was used. For the dual-energy CT, collimation was set to 14 × 1.2 mm on both detectors. For all data sets, the gantry rotation speed was 0.5 s.

DSA (TM Philips Allura, Philips Healthcare, Best, The Netherlands and Toshiba Infinix DP-i, Toshiba Medical Systems, Tokyo, Japan) was performed via a transfemoral arterial access the day after DECT. The celiac trunk and the superior mesenteric artery were explored utilizing a macro catheter (5 French Sidewinder-1-Catheter, 5 French Cobra Catheter, Terumo Europe, Leuven, Belgium). After completing overviews of the hepatic arteries a selective angiography of the left and right liver lobe was performed using a microcatheter (Rebar Microcatheter, 0.027 in; EV3, Plymouth, MN, USA) and a contrast power injection (Flow 3 ml/s, volume 12 ml, Xenetix 300™, *Guerbet, Sulzbach, Germany*).

2.3. Postprocessing and image reconstruction

Axial post-contrast images were reconstructed by using a section thickness and an increment of 3 mm. The dual-energy CT generates three different series of images: 80-kV images, 140-kV images and weighted-average images, which are based on attenuation information on images obtained from both detectors, using 70% information from the high-kVp and 30% from the low-kVp imaging. Weighted-average images are similar to 120-kVp imaging of the abdomen. Images were loaded onto a dedicated dual-energy postprocessing workstation (syngo MMWP; Siemens Medical Solutions, Forchheim, Germany).

Table 1
Attenuation values (HU) for 80-kVp and virtual 120-kV images in different anatomical regions of the abdomen.

Anatomical Region	80 kVp	virtual 120 kVp	p-value
Liver metastases	121.4 ± 13.3	96.7 ± 18.5	<0.05
Liver	70.1 ± 11.6	61.4 ± 7.6	<0.05
Muscle	47.4 ± 16.2	42.4 ± 11.0	<0.05
Fat	−111.3 ± 18.5	−92.2 ± 16.2	<0.05
Air	−957.4 ± 145.2	−982.5 ± 99.3	<0.05
Aorta	367.9 ± 73.6	233.4 ± 54.6	<0.05

2.4. Measurements of metastases and image quality

Two experienced (CT-experience 15 years and DSA-experience 10 years for both) radiologists read all the cases together. On a dedicated workstation (syngo MMWP, Siemens Medical Solutions), 3-mm CT and angiography images were displayed side by side (window width, 350 HU; window level, 50 HU). CT attenuation was determined in 7 regions using regions of interest of 0.2–1.0 cm^2 in size: hepatic metastases, normal hepatic parenchyma; aorta at the level of the coeliac trunk; psoas muscle; perihepatic fat; and air outside the patient body. For both CT image sets, the radiologists rated image noise on a five-point scale: 1, none; 2, minimal; 3, mild; 4, moderate; and 5, severe. Overall image quality was rated with a different five-point scale as follows: 1, excellent; 2, good; 3, fair; 4, poor; and 5, not diagnostic. Both readers reported all hypervascular liver metastases together for 80 kVp-, virtual-120-kVp and DSA images according to size (<10 mm; 10–20 mm; >20 mm). Follow up scans 3 and 6 months after therapy were consulted to verify and differentiate metastases against hypervasculare non metastases e.g. haemangioma.

2.5. Statistical analysis

CT-Attenuation, number of detected lesions and image quality parameters were tested for differences by using the *Wilcoxon* test for paired samples. All calculations were performed by using statistical software (SPSS, version 21, SPSS Inc., Chicago, USA). Means and standard deviations were calculated.

3. Results

3.1. Measurements of metastases

The mean attenuation values of 80 kVp- and virtual 120 kVp images for hypervascular hepatic metastases were 121.4 ± 13.3 HU and 96.7 ± 18.5 HU, respectively ($p < 0.001$). All other anatomical regions (liver, fat, aorta, muscle, air) differed significantly when the two datasets were compared (Table 1).

The mean (Table 2). number of detected lesions of all 20 patiens on 80-kVp, virtual 120-kVp and DSA images was 5.6 ± 2.1, 4.1 ± 1.8, and 4.3 ± 1.6, respectively. The differences between 80 kVp-images and virtual 120 kVp-/DSA- images were significant ($p < 0.05/p < 0.05$).

All lesions sizes were significant better detected with 80 kVp images than with virtual 120 kVp and DSA-Images (80 kVp vs. 120 kVp: <10 mm: 34 vs. 19, $p < 0.05$; 10–20 mm:, 33 vs. 25, $p < 0.05$; >20 mm: 56 vs. 42, $p < 0.05$/80 kVp vs. DSA: <10 mm: 34 vs. 18 $p < 0.05$; 10–20 mm: 33 vs. 24, $p < 0.05$; >20 mm: 56 vs. 41, $p < 0.05$).

Table 2
Number of detected hypervascular liver metastases (HLM) (mean and overall) for 80-kVp, virtual 120-kVp and DSA images with min. and max. lesion sizes.

	80 kVp	virtual 120 kVp	DSA
HLM (mean per liver)	5.6 ± 2.1	4.1 ± 1.8	4.3 ± 1.6
HLM (overall) (min.-max. size/mean size in mm)	123 (3–53/2.5 ± 2)	88 (4–53/2.6 ± 1.9)	84 (4–54/2.5 ±)

Table 3
Number of detected liver metastases according to size by each imaging technique.

Tumor Size (mm)	80 kVp images	virtual 120 kVp images	DSA
<10	34	19	18
10–20	33	25	24
>20	56	42	41

Table 4
Image quality parameters for 80-kVp and virtual 120-kVp images.

Variable	80 kVp	virtual 120 kVp	p-value
BN	13.6 ± 4.3	9.7 ± 5.4	<0.05
Subjective noise rating	3.3 ± 1.5	1.5 ± 0.4	<0.05
SNR	11.4 ± 2.6	7.7 ± 3.7	<0.05
CNR	7.5 ± 3.2	4.8 ± 2.9	<0.05
Image quality	2.8 ± 0.7	1.6 ± 0.9	<0.05

Number of detected small lesions <10 mm with 120 kVp compared to DSA-Images were significant higher (19 vs.13; $p < 0.05$), lesions 10–20 mm and >20 mm were measured statistically equal (Table 3).

3.2. Image quality

The background noise, subjective noise rating, signal-to-noise ratio, contrast-to-noise ratio and image quality of 80-kVp and virtual 120-kVp images are summarised in Table 4. Image noise, SNR and CNR were higher on 80 kVp images compared to 120 kVp images, image quality was higher on virtual 120 kVp images.

4. Discussion

The present study demonstrates that dual energy computed tomography (DECT) has great potential for detection of hepatic metastases in patients with uveal melanoma. The ability of DECT to extract basic information regarding iodine concentration and material composition has led to practical abdominal DECT applications that include the triage of patients with nephrolithasis based on stone composition, quantification of liver iron stores, evaluation of tissue perfusion, potential reduction in radiation dose by elimination of a separate unenhanced CT acquisition, and improved detection of pathologic hyperenhancement [5,12–17].

We could show that significant more and smaller metastases can be detected with the help of low kVp images compared to the virtual 120 kVp and DSA images. In a previous study we investigated the diagnostic value of DECT for detecting HCC-lesions [5]. Low kVp images in this study were also more sensitive regarding small HCC tumors. When compared with 120 kVp data, pure 80 kVp data acquired from a dual source dual energy MDCT scanner demonstrates greater attenuation differences and improved contrast to noise between metastatic disease and normal liver in an other study. In contrast to previous studies we have consulted the angiography as a sensitive investigation for comparison.

The poorer image quality of low kVp images caused by the increased image noise had no negative influence on the recognizability of metastases because sensitivity was increased by the higher SNR and CNR. In this context Hur et al. showed that the iterative reconstruction in image space algorithm yielded a significant improvement in image quality for MDCT images at low tube voltage (80 kVp) and intermediate tube current (340 mAs) setting and further may be effective for reducing patient radiation dose and for improving the conspicuity of hyperenhancing HCCs in thin adults when compared with standard 120 kVp CT images using the filtered back-projection reconstruction algorithm [18].

We could also verify a good diagnostic agreement between the angiography (DSA) of the liver and the regular used 120 kVp images of computed tomography as it has been done before by other authors [11]. But our results suggests that there is also an diagnostic advantage of the low kVp-images of DECT compared to the regular 120 kVp-images.

Cross-sectional imaging methods are the standard methods for staging of advanced melanoma. The former time-consuming and expensive multimodality approach is increasingly replaced by novel whole-body (WB) staging methods, such as 18F-fluorodeoxyglucose positron emission tomography/computed tomography (^{18}F-FDG-PET-CT) and whole-body magnetic resonance imaging (WBMRI) because they offer a complete head-to-toe coverage of the patient in a single examination with an accurate and sensitive detection of tumor spread. The preliminary results indicate a high overall diagnostic accuracy of both methods; however, these methods differ in organ-based detection rates: PET-CT was more accurate in N-staging and detection of lung and soft tissue metastases whereas WB-MRI was superior in detecting liver, bone and brain metastases [19].

Compared to PET/CT and PET/MRI DECT is less expensive and time consuming focused on detection of liver metastases, but for whole body staging DECT is inferior to the PET-methods. Another advantage of DECT compared to regular computed tomography is the decreased radiation dose because of the missing native scans.

Wagner et al. aimed to assess the sensitivity of diffusion-weighted (DW) magnetic resonance (MR) imaging for the detection of pathologically confirmed uveal melanoma liver metastases (UMLM). They showed that the addition of DW imaging to morphologic-dynamic images does not significantly increase MR sensitivities for UMLM detection [20].

As a limitation of this study histopathology was not available for the detected hypervascular liver lesions rated as metastases. However diagnosis was carried out by follow-up studies.

In conclusion, low-kVp images of DECT datasets are more sensitive in detecting liver metastases of patients with uveal melanoma than virtual 120 kVp- and DSA images.

References

[1] G. Virgili, G. Gatta, L. Ciccolallo, et al., Incidence of uveal melanoma in Europe, Ophthalmology 114 (12) (2007) 2309–2315.
[2] M. Diener-West, S.M. Reynolds, D.J. Agugliaro, et al., Development of metastatic disease after enrollment in the COMS trials for treatment of choroidal melanoma: collaborative: ocular melanoma study group report No 26, Arch. Ophthalmol. 123 (12) (2005) 1639–1643.
[3] S. Leyvraz, S. Piperno-Neumann, S. Suciu, et al., Hepatic intra-arterial versus intravenous fotemustine in patients with liver metastases from uveal melanoma (EORTC 18021): a multicentric randomized trial, Ann. Oncol. 25 (3) (2014) 742–746.
[4] T.G. Flohr, C.H. McCollough, H. Bruder, et al., First performance evaluation of a dual-source CT (DSCT) system, Eur. Radiol. 16 (2) (2006) 256–268.
[5] J. Altenbernd, T.A. Heusner, A. Ringelstein, S.C. Ladd, M. Forsting, G. Antoch, Dual-energy-CT of hypervascular liver lesions in patients with HCC: investigation of image quality and sensitivity, Eur. Radiol. 21 (4) (2011) 738–743.
[6] R. Duran, J. Chapiro, C. Frangakis, et al., Uveal melanoma metastatic to the liver: the role of quantitative volumetric contrast-enhanced MR imaging in the assessment of early tumor response after transarterial chemoembolization, Transl. Oncol. 7 (4) (2014) 447–455.
[7] T. Matsuo, Y. Ogino, K. Ichimura, T. Tanaka, M. Kaji, Clinicopathological correlation for the role of fluorodeoxyglucose positron emission tomography computed tomography in detection of choroidal malignant melanoma, Int. J. Clin. Oncol. 19 (2) (2014) 230–239.
[8] V. Orcurto, A. Denys, V. Voelter, et al., (18)F-fluorodeoxyglucose positron emission tomography/computed tomography and magnetic resonance imaging in patients with liver metastases from uveal melanoma: results from a pilot study, Melanoma Res. 22 (1) (2012) 63–69.
[9] V. Servois, P. Mariani, C. Malhaire, et al., Preoperative staging of liver metastases from uveal melanoma by magnetic resonance imaging (MRI) and fluorodeoxyglucose-positron emission tomography (FDG-PET), Eur. J. Surg. Oncol. 36 (2) (2010) 189–194.
[10] K. Young, N. Fidelman, F.Y. Yao, et al., Implications of discordant findings between hepatic angiography and cross-sectional imaging in transplant candidates with hepatocellular carcinoma, Liver Transpl. (2015).
[11] X.H. Zheng, Y.S. Guan, X.P. Zhou, et al., Detection of hypervascular hepatocellular carcinoma: comparison of multi-detector CT with digital

subtraction angiography and Lipiodol CT, World J. Gastroenterol. 11 (2) (2005) 200–203.
[12] B.M. Yeh, J.A. Shepherd, Z.J. Wang, H.S. Teh, R.P. Hartman, S. Prevrhal, Dual-energy and low-kVp CT in the abdomen, AJR Am. J. Roentgenol. 193 (1) (2009) 47–54.
[13] A. Graser, T.R. Johnson, H. Chandarana, M. Macari, Dual energy CT: preliminary observations and potential clinical applications in the abdomen, Eur. Radiol. 19 (1) (2009) 13–23.
[14] J.G. Fletcher, N. Takahashi, R. Hartman, et al., Dual-energy and dual-source CT: is there a role in the abdomen and pelvis? Radiol. Clin. North Am. 47 (1) (2009) 41–57.
[15] A.J. Chu, J.M. Lee, Y.J. Lee, S.K. Moon, J.K. Han, B.I. Choi, Dual-source, dual-energy multidetector CT for the evaluation of pancreatic tumours, Br. J. Radiol. 85 (1018) (2012) e891–e898.
[16] X. Dai, H.P. Schlemmer, B. Schmidt, et al., Quantitative therapy response assessment by volumetric iodine-uptake measurement: initial experience in patients with advanced hepatocellular carcinoma treated with sorafenib, Eur. J. Radiol. 82 (2) (2013) 327–334.
[17] C.N. De Cecco, A. Darnell, M. Rengo, et al., Dual-energy CT: oncologic applications, AJR Am. J. Roentgenol. 199 (5 Suppl) (2012) S98–S105.
[18] S. Hur, J.M. Lee, S.J. Kim, J.H. Park, J.K. Han, B.I. Choi, 80-kVp CT using Iterative Reconstruction in Image Space algorithm for the detection of hypervascular hepatocellular carcinoma: phantom and initial clinical experience, Korean J. Radiol. 13 (2) (2012) 152–164.
[19] C. Pfannenberg, N. Schwenzer, Whole-body staging of malignant melanoma: advantages, limitations and current importance of PET-CT, whole-body MRI and PET-MRI, Radiologe 55 (2) (2015) 120–126.
[20] M. Wagner, P. Mariani, F.C. Bidard, et al., Diffusion-weighted MRI for uveal melanoma liver metastasis detection, Eur. Radiol. (2015).